



CHORUS

This is the accepted manuscript made available via CHORUS. The article has been published as:

Interfaces in coexisting metals and Mott insulators

Juho Lee and Chuck-Hou Yee

Phys. Rev. B **95**, 205126 — Published 17 May 2017

DOI: [10.1103/PhysRevB.95.205126](https://doi.org/10.1103/PhysRevB.95.205126)

Interfaces in coexisting metals and Mott insulators

Juho Lee and Chuck-Hou Yee

Dept. of Physics & Astronomy, Rutgers, The State University of New Jersey, Piscataway, NJ 08854, USA

(Dated: March 13, 2017)

Motivated by the direct observation of electronic phase separation in first-order Mott transitions, we model the interface between the thermodynamically coexisting metal and Mott insulator. We show how to model the required slab geometry and extract the electronic spectra. We construct an effective Landau free energy and compute the variation of its parameters across the phase diagram. Finally, using a linear mixture of the density and double-occupancy, we identify a natural Ising order parameter which unifies the treatment of the bandwidth and filling controlled Mott transitions.

I. INTRODUCTION

The Mott transition is one of the fundamental organizing principles for understanding phases of matter in interacting solid state systems. In these materials, temperature, pressure or chemical doping drives a transition between a metal and a Mott insulator, a state where electrons cannot conduct due to the large ratio of the local Coulomb repulsion relative to the kinetic energy. The Mott transition has overwhelmingly been observed to be first-order in large classes of materials¹ and its understanding is key to eventual device applications². First-order transitions exhibit phase separation, and the thickness of the interface between the two thermodynamic phases contains information about the free energy functional³. Specifically, the thickness of the interface allows direct access to the ratio of the potential to kinetic energy terms in the free energy, which is related to the barrier height between the two minima of the double-well.

Phase separation at the Mott transition is theoretically well-studied⁴⁻⁹, establishing the coexistence between the undoped Mott insulator and a doped phase, either a normal metal or pseudogapped state. Extensive work has also examined Mott systems in inhomogeneous geometries, exploring correlated surfaces and heterostructures, where the Coulomb repulsion or hopping is varied spatially¹⁰⁻¹². Enhanced correlations are found at vacuum-facing surfaces of Mott insulators due to reduced coordination and consequent decrease in kinetic energy^{13,14}. Power law decay of the metallic quasiparticle weight as a function of distance from the interface occurs in heterostructures between metals and Mott insulators tuned to criticality^{15,16}. In contrast to electronic interfaces pinned to underlying structural inhomogeneity, the interface arising from the coexistence of metallic and Mott insulating regions in a homogeneous bulk has received little attention. The recent development of experimental probes with nanometer-scale spatial resolution¹⁷⁻¹⁹ has allowed the direct observation of the real-space structure of the metal-Mott insulator interface. Additionally, future device applications based on control of the Mott transition will also encounter these interfaces.

To characterize the metal-Mott interface, we propose a double-well form for the Landau free energy, selecting a two-component field to treat the bandwidth and doping

driven transitions simultaneously. We adapt the techniques used above for inhomogeneous correlated systems to model the real-space structure of the interface. In this work, we focus on the metallic and paramagnetic Mott insulating states in the canonical model of a correlated system, the single-band Hubbard model. The two-phase coexistence between these states is chosen because it is observed in experiment and avoids complications arising from multi-phase coexistence from the inclusion of magnetic and superconducting states. We extract the evolution of the density, double-occupancy and spectral features across the interface, allowing us to determine the parameters of the underlying Landau free energy across the phase diagram.

II. LANDAU FREE ENERGY

The Mott transition can be tuned by two parameters besides temperature: the chemical potential μ and correlation strength U . At half-filling, extensive work has shown the first-order transition is analogous to the liquid-gas transition, placing the Mott transition within the Ising universality class²⁰⁻²⁷. In this work, we extend the construction away from half-filling into the μ - U plane²⁸. Since we are interested in the metal-Mott interface, we work at temperatures below the critical point to construct the Landau functional.

We choose our fields to be the quantities conjugate to the external parameters (μ, U) , namely the density $n = \langle n \rangle$ and double occupancy $d = \langle n_{\uparrow} n_{\downarrow} \rangle$, a construction hinted at in²⁹. In first-order transitions without an organizing symmetry, any number of fields can be chosen to construct the free energy^{21,22,27}. The choice of the quantities conjugate to the physical tuning parameters μ and U allow for a transparent construction of the order parameter which can uniformly treat both the bandwidth and filling controlled transitions. Since the transition between the metal and paramagnetic Mott insulator does not break any symmetries^{1,30}, the terms in the free energy functional $\mathcal{F}[n, d]$ are unconstrained. The free energy generically will have one global minimum, and should a transition exist, it will occur via the switching between two discrete minima as no symmetry forces a locus of states to simultaneously lower in energy. We will

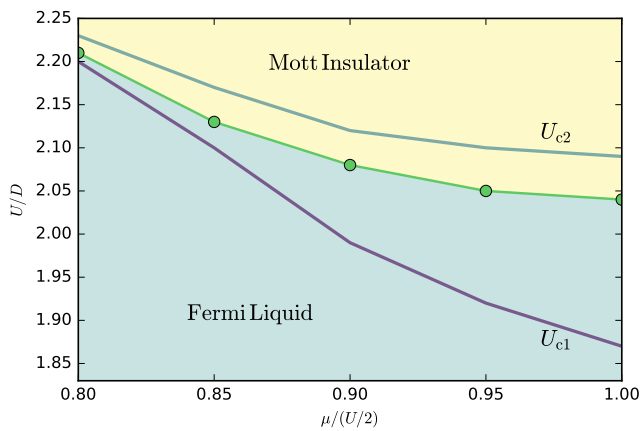


FIG. 1. Generic Mott phase diagram, as realized by the single-band Hubbard model on a cubic lattice at $T = 0.005D$, where $D = 6t$ is the half-bandwidth. Dots label values of (μ, U) lying on first-order Mott transition line used for interface calculations. Lines mark the spinodals U_{c1} and U_{c2} where the insulating and metallic solutions respectively vanish. The diagram is symmetric about $\mu/(U/2) = 1$.

explicitly construct the scalar order parameter in the following.

Along the Mott transition line in the μ - U plane, the two minima will have the same energy. To facilitate analytic calculation, we take the two minima to be symmetric, an assumption certainly not justified by symmetry, but which will prove to be a good approximation. Writing the fields as $\vec{\phi} = (n, d)$, the free energy functional takes a double-well form,

$$\mathcal{F}[\vec{\phi}] = \frac{1}{2}D(\nabla\vec{\phi})^2 + \lambda(\vec{\phi} - \vec{\phi}_i)^2(\vec{\phi} - \vec{\phi}_m)^2, \quad (1)$$

where $\vec{\phi}_i = (n_i, d_i)$ and $\vec{\phi}_m = (n_m, d_m)$ are the insulating and metallic minima. Terms beyond the quartic are certainly present and will affect the geometric shape of the potential wells. The additional parameters will improve the fit of the phenomenological free energy to the microscopic model at the expense of model complexity. We find the double well form fits sufficiently well (see Fig. 3). A note on units: we work on a discrete lattice to easily connect with computation and set the lattice spacing $a = 1$. Thus the gradient is understood to be discrete $\nabla\vec{\phi}_j \sim \vec{\phi}_{j+1} - \vec{\phi}_j$, where j is the lattice site, the free energy $F = \sum_j \mathcal{F}[\vec{\phi}_j]$, and both λ and D have units of energy. We choose D to be the half-bandwidth and omit an overall (dimensionless) normalization to the free energy.

A domain wall is given by the standard solution used, e.g. in the theory of instantons³¹,

$$\vec{\phi}(x_j) = \frac{\vec{\phi}_m + \vec{\phi}_i}{2} + \frac{\vec{\phi}_m - \vec{\phi}_i}{2} \tanh\left(\frac{x_j - x_0}{2l}\right) \quad (2)$$

where x_j is the coordinate of the j th site and the wall thickness is $l^{-2} = 2(\lambda/D)(\vec{\phi}_m - \vec{\phi}_i)^2$. The fields $\vec{\phi}$ do not

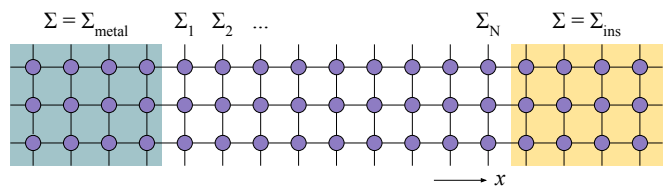


FIG. 2. Geometry used to model the metal-Mott interface. The transition region, described by site-dependent self-energies Σ_i , is sandwiched between a semi-infinite bulk Fermi liquid and Mott insulator by fixing the bulk self-energies to Σ_{metal} and Σ_{ins} on the left and right. We assume translational invariance in the y and z directions.

transform as a vector and the notation is for convenience. Determining the dependence of $\vec{\phi}_i$, $\vec{\phi}_m$ and λ/D on (U, T) requires microscopic modeling.

III. MODELING THE INTERFACE

The Hubbard hamiltonian is the “standard model” of correlated electrons. Its two terms describe the competition between kinetic energy, which delocalizes electrons to promote metallic behavior, and mutual electron repulsion, which tends to localize electrons onto sites and drive the transition to a Mott insulator. We work with the simplest one-band case on a cubic lattice,

$$H = \sum_{\mathbf{k}\sigma} (\epsilon_{\mathbf{k}} - \mu) n_{\mathbf{k}\sigma} + U \sum_j n_{j\uparrow} n_{j\downarrow}, \quad (3)$$

where we take $\epsilon_{\mathbf{k}} = -2t(\cos k_x + \cos k_y + \cos k_z)$ and use the half bandwidth $D = 6t$ as the unit of energy in all the following. We will index the sites by $j = (n_1, n_2, n_3)$ in the following. Ignoring ordered phases, which is a reasonable assumption at intermediate temperatures or in the presence of frustration, the phase diagram generically consists of a Mott insulating region for large U and a range of μ corresponding to half-filling, and a Fermi liquid everywhere else. To find the first-order transition line, we use standard single-site dynamical mean-field theory (DMFT)^{32–34} with a continuous-time quantum monte carlo (CTQMC) hybridization expansion impurity solver^{35–37}. The phase diagram at $T = 0.005D$ is plotted in Fig. 1, along with the two spinodals U_{c1} and U_{c2} between which both solutions exist.

To model the interface in the coexistence regime, we fix our parameters to a point on the first-order line (dots in Fig. 1), then partition the lattice into three regions along the x -axis (see Fig. 2): metal ($n_1 \leq 0$), insulator ($n_1 \geq N+1$), and a *transition* region ($1 \leq n_1 \leq N$). Here n_1 is the site index along the x -axis and we take $N = 20$ large enough to capture the interface. We perform an inhomogenous DMFT calculation by setting the self-

energy of the lattice $\Sigma_{n_1 n'_1} = \delta_{n_1 n'_1} \Sigma_{n_1}$ to

$$\Sigma_{n_1} = \begin{cases} \Sigma_{\text{metal}} & n_1 \leq 0 \\ \Sigma_{n_1} & 1 \leq n_1 \leq N \\ \Sigma_{\text{ins}} & n_1 \geq N + 1 \end{cases} \quad (4)$$

Only the self-energies Σ_{n_1} in the transition region are updated, while Σ_{metal} and Σ_{ins} are fixed boundary conditions taken from the single-site DMFT solution. Our setup assumes the interface is perpendicular to one of the crystal directions (x) and the system is translationally invariant in the other two (y and z) so self-energies are independent of n_2 and n_3 .

To render the equations soluble in the transition region, we compute the lattice Green's function and use its local component $G_{n_1 n_1}$ to map the system to a chain of N auxiliary impurity problems¹²,

$$G_{n_1 n_1}(i\omega_n) = \frac{1}{i\omega_n - E_{\text{imp}} - \Delta_{n_1}(i\omega_n) - \Sigma_{n_1}(i\omega_n)}. \quad (5)$$

Using the extracted impurity levels E_{imp} and hybridization functions Δ_{n_1} , we obtain the new local self-energies Σ_{n_1} and iterate to convergence. The procedure for computing the local Green's function is provided in the appendix.

IV. RESULTS

The evolution of the density n and double occupancy d across the interface as we progress along the Mott transition line is displayed in Fig. 3. The temperature is fixed to $T = 0.005D$. The position along the transition line (see Fig. 1) is parameterized by μ , as labeled in the figure, and the corresponding U is tabulated in the right side of Table I. The fact that the system equilibrates to a finite interface width, rather than linearly interpolating between the endpoints, implies there exists an intrinsic scale, which is controlled by the double well height. The results remain unchanged with transition regions up to 60 sites in width, demonstrating convergence of the interface (see appendix). The lack of finite size effects can also be visually seen by the flat plateaus in n and d on either side of the interface. As expected, the insulator is more ‘‘rigid’’ compared to the metal: both n and d shift less on the insulating (right) side of the figure as μ is varied.

Appealing to intuitively expected properties of the metal and insulator, the variations of n and d across the interface can be rationalized. In the upper plot of density, at the particle-hole symmetric point of $\mu = 1.0(U/2)$, there is no jump in density between the metal and Mott insulator as they both lie at half filling. As μ is decreased, the metallic density drops due to the finite compressibility of the phase. At zero temperature, the insulating density would be exactly pinned at unity regardless of variations in μ . However, the simulations were performed at finite temperature, the insulator has a small

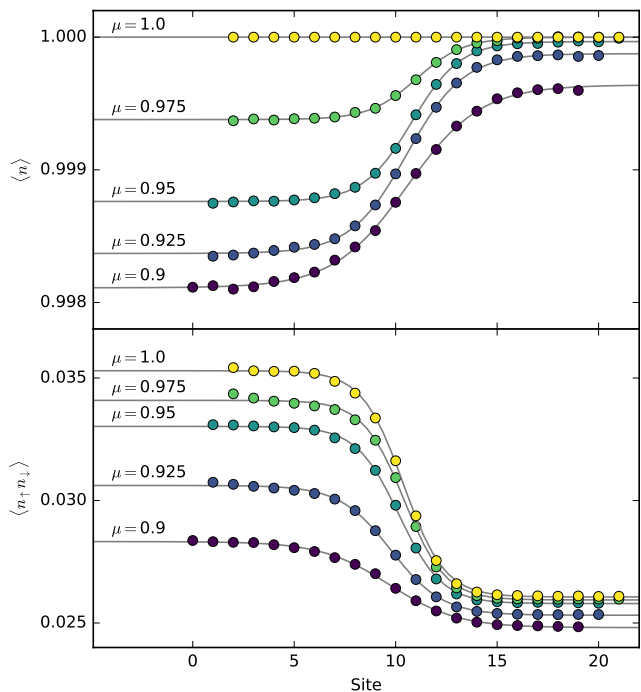


FIG. 3. Variation of the density (top) and double occupancy (bottom) across the interface at several points along the Mott transition line at $T = 0.01D$. Thin lines are fits to the standard solution for a double-well potential $a + b \tanh((x_i - x_0)/2l)$, allowing extraction of the parameters for the underlying free energy. Curves are shifted horizontally by varying amounts to align the center of the domain wall for clarity (0, 1, 1, 2, 2 sites respectively). The chemical potential is in units of $U/2$, as detailed in the right-hand table of Table I

but finite compressibility, resulting in a small drop in density below unity. As a result, the density difference between the metal and insulator increases as we progress along the transition line.

In the lower plot of the double occupancy, we find the jump is maximal at the particle-hole symmetric point. Since stepping along the Mott transition line away from the $\mu = 1.0(U/2)$ point involves increasing U , the double occupancy is reduced in both the metal and insulator by the enhanced correlations. Again, the metal is more compressible, exhibiting a larger drop in d . As a result, the difference in double occupancy decreases as we progress along the transition line.

The variation of both quantities fit well to Eq. 2 for the double well potential, albeit with slightly different length scales, and we use the average of the two wall widths l to compute λ . The small difference in length scales implies the potential is not perfectly symmetric, and that the path in (n, d) space between the two minima is close to, but not exactly, a straight line (see Fig. 4). The extracted parameters for the Landau free energy are presented in Table I. The width of the domain wall increases as we move away from the particle-hole symmetric point. We hypothesize this is due to the lowering in temperature of

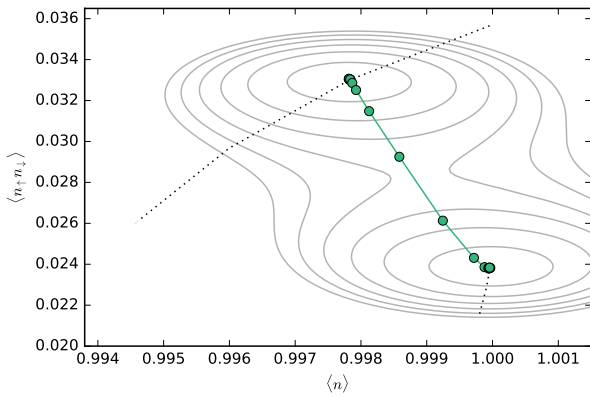


FIG. 4. Trajectory in (n, d) space as the system evolves across the interface from the insulating to the metallic minima at $\mu = 0.95(U/2)$, $U = 2.05D$, $T = 0.005D$. The extracted Landau parameters are used to plot the contours of the double-well potential. The dotted lines trace the shift of the minima along the Mott transition line at $T = 0.005D$.

the Mott critical end point with increasing U , and length scales are expected to diverge as our parameters move the system closer to the critical point.

We also analytically continue the Matsubara self-energies produced by the impurity solver to the real axis using the maximum entropy method³⁸ to compute the variation of the spectral density across the interface. We plot in Fig. 5 the spectra for parameters $\mu = 0.95(U/2)$, $U = 1.97D$ and $T = 0.01D$, which is slightly on the hole-doped side. Starting from the metallic solution, we find that the quasiparticle peak shifts slightly downwards and disappears into the lower Hubbard band as we progress to the Mott insulator. The gap between the Hubbard bands slightly narrows. The shift in the quasiparticle peak is challenging to see, so also plotted in the appendix is a comparison between the line spectra of the first and last sites in the transition region. Additionally, we use $G(\beta/2)$ to independently check the quasiparticle weight at the Fermi level (see appendix). In corroboration with the analytically continued results, we find the weight to be finite on the metallic side, decreases as the interface is traversed, and approaches zero on the insulating side.

The extracted parameters combined with our ansatz (Eq. 1) allow us to reconstruct the free energy. A representative case for $\mu = 0.95$, $U = 2.05$, $T = 0.005D$ is shown in Fig. 4. We have plotted the trajectory in (n, d) space as the system evolves from the metallic to insulating minima, superimposed with contour lines of the potential constructed using the extracted parameters. The movement of the two minima as we step along the Mott transition line is shown in the dotted lines.

As promised, we explicitly construct the order parameter field Δ as a linear combination of n and d , owing to the fact that the trajectory is almost straight. The construction is essentially geometric: we take the line segment joining the two minima and parameterize it with

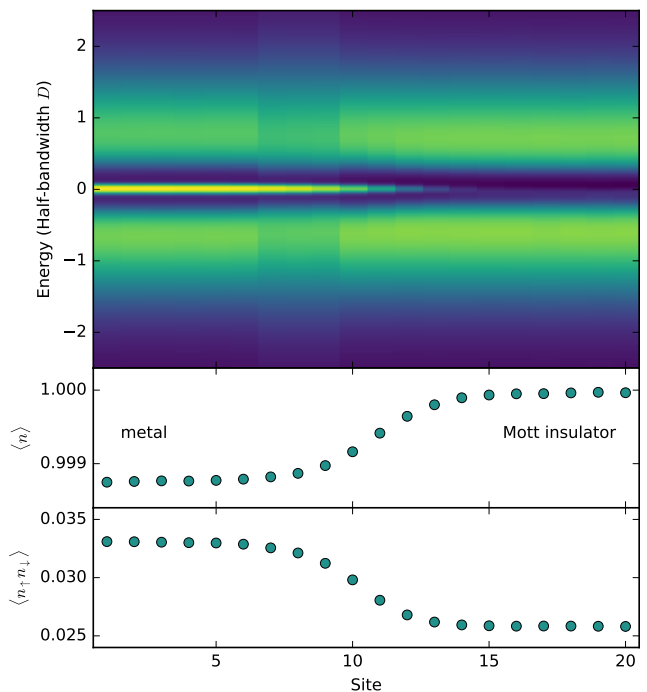


FIG. 5. Evolution of the local spectra (top panel), density (middle) and double occupancy (bottom) across the interface between a correlated metal (left edge) and a Mott insulator (right edge). Visible is the transfer of spectral weight from the low-energy quasiparticles to the Hubbard bands as we spatially traverse the interface (light color corresponds to high spectral density, and dark to low density). We have chosen parameters of the Hubbard model where the transition from the insulator is to a hole-doped metal: $\mu = 0.95(U/2)$, $U = 1.97D$ and $T = 0.01D$, where $D = 6t$ is the half-bandwidth.

an angle α :

$$\Delta = (n - \bar{n}) \sin \alpha + (d - \bar{d}) \cos \alpha \quad (6)$$

where $\bar{n} = (n_i + n_m)/2$ and $\bar{d} = (d_i + d_m)/2$. The angles are tabulated in Table I. At particle-hole symmetry, the angle is zero and the variation of the order parameter is entirely driven by the double occupancy. Increasing angles imply that the density becomes a larger component of the order parameter, which occurs as we progress to larger correlation strengths.

V. SUMMARY

In this work, we have taken a preliminary step towards characterizing the metal-Mott interface by modeling its spatial properties, constructing a Landau free energy and identifying an Ising order parameter. The key parameter of the free energy which could not be obtained by previous solutions in uniform systems is the interface width l , which is directly related to the double-well barrier height via λ/D .

$\mu/(U/2)$	U/D	n_i	d_i	n_m	d_m	\bar{l}	λ/D	α
1.00	2.04	1.0000	0.0241	1.0000	0.0357	0.72	2410	0°
0.95	2.05	1.0000	0.0238	0.9978	0.0330	0.75	3170	13°
0.90	2.08	0.9999	0.0229	0.9960	0.0297	0.80	2510	30°
0.85	2.13	0.9998	0.0216	0.9947	0.0262	1.04	1780	48°

$\mu/(U/2)$	U/D	n_i	d_i	n_m	d_m	\bar{l}	λ/D	α
1.000	1.962	1.0000	0.0261	1.0000	0.0353	1.02	1420	0°
0.975	1.965	1.0000	0.0259	0.9997	0.0341	1.09	1590	2°
0.950	1.970	1.0000	0.0258	0.9994	0.0330	1.12	1890	5°
0.925	1.985	0.9999	0.0253	0.9992	0.0306	1.33	2480	8°
0.900	2.005	0.9998	0.0248	0.9991	0.0283	1.74	3190	12°

TABLE I. Extracted parameters of Landau free energy for $T = 0.005D$ (left) and $T = 0.01D$ (right), where $D = 6t$ is the half-bandwidth. The position along the Mott transition line is parameterized by the chemical potential μ , or equivalently, the electron repulsion. The shifts in the density and double-occupancy for the Mott insulator (n_i, d_i) and metal (n_m, d_m) are quite small for the one-band model, which when combined with fact that the interface widths $\bar{l} \sim O(1)$, produces large values of λ/D . The angle α specifies how much of n is admixed into the d to form the Ising order parameter (see Eq. 6).

We want to point out the simplifying assumptions used: (1) we took the interface to be perpendicular to a crystallographic axis, (2) we only included nearest-neighbor hopping to simplify the formulae, (3) we made the slow-varying approximation, assuming each site was an independent impurity affecting the others only via the hybridization, and (4) we have ignored the long-range Coulomb interaction. Relaxing these assumptions to capture more realistic scenarios warrants further investigation. In particular, while the long-range Coulomb interaction primarily controls the domain sizes of the metallic and Mott insulating puddles via the competition between the surface tension and bulk Coulomb energy⁹, its effects on the interface width are likely more subtle and require detailed modeling. Additionally, since this was a first study, we believe it is appropriate to examine the phenomenon in the Hubbard model before progressing to chemically realistic models, where the essential physics would be complicated by effects such as Glazer rotations in perovskites, multi-band physics, and Hund's coupling.

Additionally, while forbidding ordered phases (especially magnetism) in the calculations is roughly valid for modeling the Mott transition at finite temperatures, a more detailed study would include order parameter fluctuations. For example, including magnetic correlations would lower the entropy of the paramagnetic Mott insulator relative to the metal. This shift in relative entropy changes the slope of the Mott transition surface to increasingly favor the metal at higher temperatures³⁹, and will affect the extracted free energy parameters.

We expect that future calculations on realistic systems will provide quantitative results for comparison with near-field optics and STM observations. More speculatively, these calculations could provide a new constraint on the value of U in Mott compounds such as the rare earth titanates, vanadium oxides and organics. Finally, while we have made an ansatz for the form of the Landau free energy and numerically determined its parameters, especially satisfying for future work would be a microscopic derivation from the appropriate mean-field theory.

VI. ACKNOWLEDGEMENTS

C.Y. thanks Patrick Semon, Camille Aron, Premala Chandra, and Gabriel Kotliar for stimulating discussions, and Leon Balents, whose thermodynamic construction of the Mott transition inspired this work. C.Y. was supported as part of the Center for Emergent Superconductivity, an Energy Frontier Research Center funded by the US Department of Energy, Office of Science, Office of Basic Energy Sciences under Award No. DEAC0298CH1088. J.L. acknowledges support from the Rutgers Physics Departmental Fellowship.

Appendix A: Calculation of local Green's function

The Green's function of the lattice is given by

$$G_{\mathbf{R}\mathbf{R}'} = [(i\omega + \mu)\delta_{\mathbf{R}\mathbf{R}'} - t_{\mathbf{R}\mathbf{R}'} - \Sigma_{\mathbf{R}\mathbf{R}'}]^{-1} \quad (\text{A1})$$

where \mathbf{R} is a lattice vector $\mathbf{R} = (n_1, n_2, n_3)$ with the cubic primitive lattice vector and $t_{\mathbf{R}\mathbf{R}'}$ denotes the nearest neighbor hopping. To see the spatial variation across the two different phases, we divide the lattice into three regions: metallic ($\mathcal{M} : -\infty < n_1 \leq 0$), insulating ($\mathcal{I} : N + 1 \leq n_1 < \infty$) and transition ($\mathcal{T} : 1 \leq n_1 \leq N$) region. So \mathcal{T} is sandwiched by \mathcal{M} and \mathcal{I} . Then we assign to each site the localized self-energy $\Sigma_{n_1 n'_1} = \delta_{n_1 n'_1} \Sigma_{n_1}$ with

$$\Sigma_{n_1} = \begin{cases} \Sigma_{\text{metal}} & (n_1 \in \mathcal{M}) \\ \Sigma_{n_1} & (n_1 \in \mathcal{T}) \\ \Sigma_{\text{ins}} & (n_1 \in \mathcal{I}) \end{cases} \quad (\text{A2})$$

Note that in the metallic and insulating regimes, the self-energy is fixed to Σ_{metal} and Σ_{ins} respectively, while we allow the local self-energy in the transition regime to vary across the sites.

The Fourier transformation of Eq. (A1) along y and z directions gives the following matrix form of Green's function in the mixed representation $(n_1; k_y, k_z)$ (n_1 is

the site index of x):

$$[G(k_y, k_z; i\omega)]_{n_1 n'_1} = \left[\begin{array}{c} [(i\omega + \mu - \varepsilon(k_y, k_z) - \Sigma_{n_1}(i\omega))\hat{I} - \hat{t}]^{-1} \end{array} \right]_{n_1 n'_1} \quad (\text{A3})$$

where $\hat{t} = -t(\delta_{n_1, n'_1+1} + \delta_{n_1, n'_1-1})$ and $\varepsilon(k_y, k_z) = -2t(\cos(k_y a) + \cos(k_z a))$. To apply DMFT to the transition regime, we must calculate the local component of the Green's function at each site and map each onto an auxiliary impurity.

We can rewrite Eq. (A3) in a block matrix divided into the three regimes \mathcal{M} , \mathcal{T} and \mathcal{I} , that is,

$$[G(k_y, k_z; i\omega)]_{n_1 n'_1} = \left[\begin{array}{c|c|c} F_{\mathcal{M}} & t & \\ \hline & t & F_{\mathcal{T}} \\ \hline & & t \end{array} \right]^{-1} \quad (\text{A4})$$

$$[G(k_y, k_z)]_{n_1, n'_1 \in \mathcal{T}} = \underbrace{\left[\begin{array}{c} F_{\mathcal{I}} \\ \hline \end{array} \right]}_{\mathbf{A}} - \underbrace{\left(\hat{t}_{\mathcal{T}\mathcal{M}} [F_{\mathcal{M}}]^{-1} \hat{t}_{\mathcal{M}\mathcal{T}} + \hat{t}_{\mathcal{T}\mathcal{I}} [F_{\mathcal{I}}]^{-1} \hat{t}_{\mathcal{I}\mathcal{T}} \right)}_{\mathbf{B}\mathbf{D}^{-1}\mathbf{C}}^{-1}$$

$$= \left[\begin{array}{ccc|ccc} z_{11} - t^2 R_{\mathcal{M}} & t & & & & 0 \\ & t & z_{22} & t & & \\ & & t & \ddots & \ddots & \\ & & & \ddots & \ddots & t \\ & & & & t & z_{N-1, N-1} \\ 0 & & & & t & z_{NN} - t^2 R_{\mathcal{I}} \end{array} \right]^{-1} \quad (\text{A6})$$

where $R_{\mathcal{M}} \equiv [F_{\mathcal{M}}^{-1}]_{00}$, $R_{\mathcal{I}} \equiv [F_{\mathcal{I}}^{-1}]_{N+1, N+1}$ and $\hat{t}_{\mathcal{T}\mathcal{M}(\mathcal{I})}$ is the overlap between \mathcal{T} and $\mathcal{M}(\mathcal{I})$. The effect of integrating out the degrees of freedom in \mathcal{M} and \mathcal{I} is captured by $t^2 R_{\mathcal{M}}$ and $t^2 R_{\mathcal{I}}$ at the $(1, 1)$ and (N, N) components respectively.

To compute $R_{\mathcal{M}}$ and $R_{\mathcal{I}}$, we again rely on Eq. (A5). Since $[F_{\mathcal{M}}]$ takes a symmetric tridiagonal matrix form equal to

$$F_{\mathcal{M}} = \left[\begin{array}{c|c} z_{\mathcal{M}} & t \\ \hline t & z_{\mathcal{M}} & t \\ & t & z_{\mathcal{M}} & \ddots \\ & & \ddots & \ddots \end{array} \right] = \left[\begin{array}{c|c} z_{\mathcal{M}} & t \\ \hline t & F_{\mathcal{M}} \end{array} \right] \quad (\text{A7})$$

we see the matrix repeats itself inside. As a direct consequence of (A5), we obtain the following recursive equa-

where we define the three block matrices by

$$[F_{\mathcal{M}}]_{n_1 n'_1} = \underbrace{(i\omega + \mu - \varepsilon(k_y, k_z) - \Sigma_{\mathcal{M}}(i\omega))}_{\equiv z_{\mathcal{M}}} \delta_{n_1 n'_1} - t_{n_1 n'_1}$$

$$[F_{\mathcal{T}}]_{n_1 n'_1} = \underbrace{(i\omega + \mu - \varepsilon(k_y, k_z) - \Sigma_{n_1}(i\omega))}_{\equiv z_{n_1}} \delta_{n_1 n'_1} - t_{n_1 n'_1}$$

$$[F_{\mathcal{I}}]_{n_1 n'_1} = \underbrace{(i\omega + \mu - \varepsilon(k_y, k_z) - \Sigma_{\text{ins}}(i\omega))}_{\equiv z_{\mathcal{I}}} \delta_{n_1 n'_1} - t_{n_1 n'_1}.$$

Note that $z_{\mathcal{M}}$ and $z_{\mathcal{I}}$ are fixed while z_{n_1} varies across the sites.

Using block matrix inversion

$$\left[\begin{array}{c|c} \mathbf{A} & \mathbf{B} \\ \hline \mathbf{C} & \mathbf{D} \end{array} \right]^{-1} \Big|_{\in \mathbf{A}} = [\mathbf{A} - \mathbf{B}\mathbf{D}^{-1}\mathbf{C}]^{-1} \quad (\text{A5})$$

we obtain the complete form of Green's function in the transition regime \mathcal{T} (a $N \times N$ matrix) into which all the degrees of freedom of metallic and insulating regions are incorporated:

tion:

$$[F_{\mathcal{M}}^{-1}]_{00} = R_{\mathcal{M}} = \frac{1}{z_{\mathcal{M}} - t^2 R_{\mathcal{M}}} \quad (\text{A8})$$

where the solution is

$$R_{\mathcal{M}} = \frac{z_{\mathcal{M}} - \sqrt{(z_{\mathcal{M}})^2 - 1}}{t}. \quad (\text{A9})$$

$R_{\mathcal{I}}$ is obtained by the same procedure.

Finally, we need to convert the mixed representation form (A4) into the pure real-space representation. Performing the inverse Fourier transformation with respect to k_y and k_z , we can obtain the local Green's function at the site n_1

$$[G]_{n_1 n_1} = \int \frac{d^2 k}{(2\pi)^2} [G(k_y, k_z)]_{n_1 n_1}$$

$$= \int d\varepsilon [G(\varepsilon)]_{n_1 n_1} D^{2D}(\varepsilon) \quad (\text{A10})$$

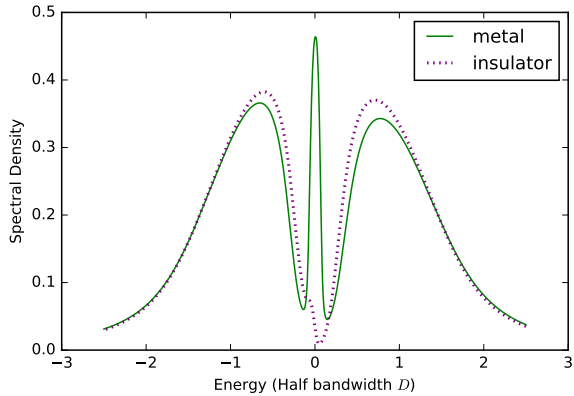


FIG. 6. Plot of the local spectra $G_n(\omega)$ for n equal to the first and last sites in the transition region (nearest the metal and insulating bulks, respectively). The quasiparticle peak is seen to shift downwards in the lower Hubbard band, and the gap between the Hubbard bands have narrowed.

where the ε dependence of G comes from $\varepsilon = \varepsilon(k_y, k_z)$. Here, $D^{2D}(\varepsilon)$ is the density of states of non-interacting 2D square lattice whose analytic expression is known and the integration (A10) is performed numerically.

Appendix B: Supplementary Plots

To show the narrowing of the Hubbard bands and shift of the quasiparticle peak downwards as the interface is traversed, we plot the local spectra of the first and last sites in the transition region in Fig. 6

As a check on the analytic continuation results, we have plotted $G(\beta/2)$ in Fig. 7, which is approximately proportional to the Fermi level density of states. The density is finite on the metallic side, and drops to zero on the insulating side of the interface.

Finally, we check for finite size effects by performing calculations for transition regions up to width $N = 60$. In Fig. 8, we show a comparison of the computed double occupancy across the interface for transition regions of size $N = 20$ and $N = 60$, at $T = 0.01D$, $\mu = 0.95(U/2)$ and $U = 1.97D$. The interface is well-captured for simulation systems of width $N = 20$.

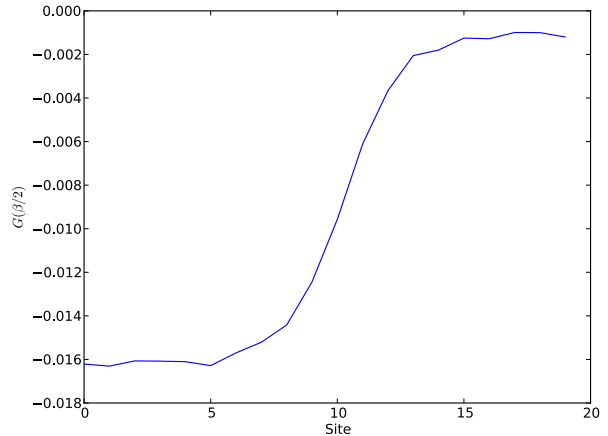


FIG. 7. Plot of $G(\beta/2)$ vs. site, showing the decrease in Fermi level density as we cross the interface from the metallic (left) to insulating (right) side.

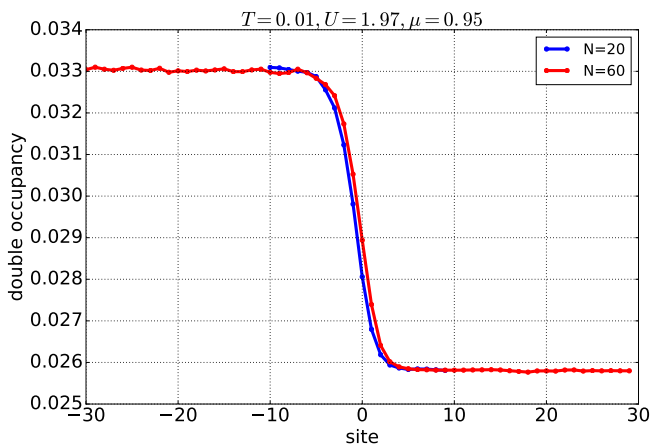


FIG. 8. Comparison of double-occupancy across the interface for transition regions of width $N = 20$ and $N = 60$.

-
- ¹ M. Imada, A. Fujimori, and Y. Tokura, *Reviews of Modern Physics* **70**, 1039 (1998).
- ² Y. Zhou and S. Ramanathan, *Critical Reviews in Solid State and Materials Sciences* **38**, 286 (2013), arXiv:1212.2684.
- ³ K. Binder, *Reports on Progress in Physics* **50**, 783 (1987).
- ⁴ P. Visscher, *Physical Review B* **10**, 943 (1974).
- ⁵ V. Emery, S. Kivelson, and H. Lin, *Physical Review Letters* **64**, 475 (1990).
- ⁶ L. Gohlhoff, *Journal of Physics: Condensed Matter* **8**, 2851 (1996).
- ⁷ S. White and D. Scalapino, *Physical Review B* **61**, 6320 (2000).
- ⁸ D. Galanakis, E. Khatami, K. Mielson, a. Macridin, J. Moreno, D. a. Browne, and M. Jarrell, *Philosophical transactions. Series A, Mathematical, physical, and engineering sciences* **369**, 1670 (2011).
- ⁹ C.-h. Yee and L. Balents, *Physical Review X* **5**, 021007 (2015), arXiv:1407.0368.
- ¹⁰ J. K. Freericks, *Physical Review B - Condensed Matter and Materials Physics* **70**, 1 (2004), arXiv:0408226 [cond-mat].
- ¹¹ H. Zenia, J. K. Freericks, H. R. Krishnamurthy, and T. Pruschke, *Physical Review Letters* **103**, 1 (2009).
- ¹² P. Bakalov, D. Nasr Esfahani, L. Covaci, F. M. Peeters, J. Tempere, and J. P. Locquet, *Physical Review B - Condensed Matter and Materials Physics* **93**, 1 (2016), arXiv:1503.02502.
- ¹³ S. Schwieger, M. Potthoff, and W. Nolting, *Physical Review B* **67**, 8 (2003), arXiv:0302427 [cond-mat].
- ¹⁴ H. Ishida, D. Wortmann, and A. Liebsch, *Physical Review B* **73**, 245421 (2006).
- ¹⁵ R. Helmes, T. Costi, and a. Rosch, *Physical Review Letters* **101**, 066802 (2008).
- ¹⁶ G. Borghi, M. Fabrizio, and E. Tosatti, *Physical Review B - Condensed Matter and Materials Physics* **81**, 1 (2010), arXiv:0911.0718.
- ¹⁷ T. Hanaguri, Y. Kohsaka, K. Iwaya, S. Satow, K. Kitazawa, H. Takagi, M. Azuma, and M. Takano, *Physica C: Superconductivity and its Applications* **408-410**, 328 (2004).
- ¹⁸ M. M. Qazilbash, M. Brehm, B.-G. Chae, P.-C. Ho, G. O. Andreev, B.-J. Kim, S. J. Yun, A. V. Balatsky, M. B. Maple, F. Keilmann, H.-T. Kim, and D. N. Basov, *Science (New York, N.Y.)* **318**, 1750 (2007).
- ¹⁹ Y. Kohsaka, T. Hanaguri, M. Azuma, M. Takano, J. C. Davis, and H. Takagi, *Nature Physics* **8**, 1 (2012).
- ²⁰ C. Castellani, C. Di Castro, D. Feinberg, and J. Ranninger, *Physical Review Letters* **43**, 1957 (1979).
- ²¹ G. Kotliar, E. Lange, and M. Rozenberg, *Physical review letters* **84**, 5180 (2000).
- ²² S. Onoda and N. Nagaosa, *Journal of the Physical Society of Japan* **72**, 2445 (2003).
- ²³ P. Limelette, A. Georges, D. Jérôme, and P. Wzietek, *Science* **302**, 89 (2003).
- ²⁴ F. Kagawa, K. Miyagawa, and K. Kanoda, *Nature* **436**, 534 (2005), arXiv:0603064 [cond-mat].
- ²⁵ S. Papanikolaou, R. M. Fernandes, E. Fradkin, P. W. Phillips, J. Schmalian, and R. Sknepnek, *Physical Review Letters* **100**, 1 (2008), arXiv:0710.1627.
- ²⁶ P. Sémon and a.-M. S. Tremblay, *Physical Review B* **85**, 201101 (2012).
- ²⁷ J. Vučićević, H. Terletska, D. Tanasković, and V. Dobrosavljević, *Physical Review B - Condensed Matter and Materials Physics* **88**, 1 (2013).
- ²⁸ P. Werner and A. Millis, *Physical Review B* **75**, 085108 (2007).
- ²⁹ M. Imada, *Physical Review B - Condensed Matter and Materials Physics* **72**, 1 (2005), arXiv:0506468 [cond-mat].
- ³⁰ D. B. McWhan and J. P. Remeika, *Physical Review B* **2**, 3734 (1970).
- ³¹ A. I. Vainshtein, V. I. Zakharov, V. A. Novikov, and M. A. Shifman, *Soviet Physics Uspekhi* **25**, 195 (1982).
- ³² W. Metzner and D. Vollhardt, *Physical Review Letters* **62**, 324 (1989), arXiv:arXiv:1011.1669v3.
- ³³ A. Georges and G. Kotliar, *Physical Review B* **45**, 6479 (1992).
- ³⁴ A. Georges, G. Kotliar, W. Krauth, and M. J. Rozenberg, *Reviews of Modern Physics* **68**, 13 (1996).
- ³⁵ P. Werner, A. Comanac, L. de' Medici, M. Troyer, and A. Millis, *Physical Review Letters* **97**, 076405 (2006).
- ³⁶ K. Haule, *Physical Review B* **75**, 155113 (2007).
- ³⁷ E. Gull, A. J. Millis, A. I. Lichtenstein, A. N. Rubtsov, M. Troyer, and P. Werner, *Reviews of Modern Physics* **83**, 349 (2011).
- ³⁸ M. Jarrell and J. E. Gubernatis, *Physics Reports* **269**, 133 (1996).
- ³⁹ H. Park, K. Haule, and G. Kotliar, *Physical Review Letters* **101**, 186403 (2008).